TITLE

Sustained Decline of Annual Snow Cover Area in the Sikkim Himalaya (1987–2025): Multi-Sensor Remote Sensing on Google Earth Engine, Machine Learning, and Projections to 2100

AUTHOR

Prakash Pradhan

AFFILIATION

West Bengal Biodiversity Board, Prani Sampad Bhawan, 5th Floor, LB-2, Salt Lake, Sector-III, Kolkata – 700106, West Bengal, India

CORRESPONDENCE

shresthambj@gmail.com

Sustained Decline of Annual Snow Cover Area in the Sikkim Himalaya (1987–2025): Multi-Sensor Remote Sensing on Google Earth Engine, Machine Learning, and Projections to 2100

PRAKASH PRADHAN[♥]

[1]West Bengal Biodiversity Board, Prani Sampad Bhawan, 5th Floor, LB-2, Salt Lake, Sector-III, Kolkata, PIN – 700106, West Bengal, India.

[♥]email: shresthambj@gmail.com

Abstract. Snow cover is a critical component of the Himalayan cryosphere, providing freshwater to millions of people across South Asia and regulating regional climate through albedo feedbacks. Sikkim, a small but ecologically significant state in the Eastern Himalaya, has experienced accelerating glacial retreat and mounting hydrological stress in recent decades. This study presents a comprehensive, multi-decadal analysis of annual snow cover area (SCA) in Sikkim from 1987 to 2025, utilising cloud-masked, cloud-free median composites derived from Landsat 5, Landsat 8, and Sentinel-2 satellite imagery processed on the Google Earth Engine (GEE) cloud computing platform. The Normalised Difference Snow Index (NDSI) threshold of 0.1 was applied uniformly across all sensors and years to map annual SCA at 30-metre spatial resolution. After quality-controlled exclusion of five years with zero valid satellite acquisitions (1984–1986, 2002, and 2012), a final time series of 37 annual observations was analysed. Results reveal a statistically significant and robust long-term decline in SCA (Mann–Kendall $z = -4.49$, $p < 0.001$; Sen's slope = −17.62 km²/year), representing an estimated cumulative loss of approximately 669 km² over the study period. Decadal mean SCA declined monotonically from 1537.75 ± 342.55 km² in the 1990s to 923.22 ± 166.44 km² in the 2020s, a 40% reduction. Six machine learning and statistical models were evaluated via Leave-One-Out Cross-Validation (LOOCV): Support Vector Regression (SVR) achieved the best performance (RMSE = 237.19 km², R^2 = 39.4%). An inverse-RMSE weighted ensemble of LM, GAM, and SVR projects a continued decline to approximately −256 km² by 2100 under the central scenario (95% PI: −1194 to +937 km²), implying functional disappearance of annual snow cover before the end of the century under business-as-usual warming. These findings provide a quantitative, long-term baseline for cryospheric change in the Eastern Himalaya, with direct relevance to water resource planning, hydrological impact assessment, and climate adaptation policy for the Teesta Basin and downstream communities.

Key words: Snow cover area; Normalised Difference Snow Index; Eastern Himalaya; Sikkim; Landsat; Sentinel-2; Google Earth Engine; Mann–Kendall trend; Machine learning; Future projections

Abbreviations: ANOVA: Analysis of Variance; BIC: Bayesian Information Criterion; CI: Confidence Interval; CV: Coefficient of Variation; EH: Eastern Himalayas; GAM: Generalised Additive Model; GBM: Gradient Boosting Machine; GCM: General Circulation Model/Global Climate Model; GEE: Google Earth Engine; GLAD ARD: Global Land Analysis and Discovery Analysis Ready Data; GLOF: Glacial Lake Outburst Flood; HKH: Hindu Kush Himalaya; ICA: Independent Component Analysis; ICIMOD: International Centre for Integrated Mountain Development; IPCC AR6: Intergovernmental Panel on Climate Change, Sixth Assessment Report; KH: Karakoram and Himalayan; LM: Linear Regression; LOOCV: Leave-One-Out Cross-Validation; LSTM: Long Short-Term Memory; MAE: Mean Absolute Error; MK: Mann–Kendall; MODIS: Moderate Resolution Imaging Spectroradiometer; NDSI: Normalised Difference Snow Index; NDSTI: Normalised Difference Snow Thermal Index; NSE: Nash–Sutcliffe Efficiency; OLI: Operational Land Imager; OLS: Ordinary Least Squares; PCA: Principal Component Analysis; PELT: Pruned Exact Linear Time; PI: Prediction Interval; PIs: Prediction Intervals; PSI: Perennial Snow Index; R^2: Coefficient of Determination; RBF: Radial Basis Function; RF: Random Forest; RMSE: Root Mean Square Error; S3: Snow Cover Index; SCA: Snow Cover Area; SR: Surface Reflectance; SVR: Support Vector Regression; SWIR: Shortwave Infrared; TM: Thematic Mapper; TWS: Terrestrial Water Storage; XGBoost: Extreme Gradient Boosting.

Running title: Snow Cover Decline in Sikkim, Eastern Himalaya (1987–2025)

INTRODUCTION

The Hindu Kush Himalaya (HKH) region, often referred to as the 'Third Pole', constitutes the world's largest store of freshwater outside the polar ice caps and sustains the livelihoods of approximately 3.3 billion people across eleven countries in its river basins (Immerzeel et al. 2010; Bolch et al. 2019; Khan et al. 2024; IPCC 2022). The Himalayan cryosphere, consisting of glaciers, seasonal snowpack, and permafrost, serves as a critical regulator of river discharge, regional albedo, and monsoon dynamics (Barnett et al. 2005; Immerzeel et al. 2020). Under ongoing anthropogenic climate change, the HKH has warmed at nearly twice the global average rate, with projected further warming of 1.5–2.5°C by mid-century under medium emission scenarios (Krishnan et al. 2019; Shrestha and Aryal 2011). This accelerated warming is driving glacier retreat and earlier, reduced seasonal snowmelt, with profound downstream hydrological consequences (Lutz et al. 2014; Kääb et al. 2012). Recent quantification of cryospheric change is unambiguous: Khan et al. (2024) used 30-metre Landsat Analysis Ready Data across the entire Hindu Kush Himalaya to show that the region lost a net 15,770 km² of perennial snow and ice from 2001 to 2021, equivalent to about one-eighth of its 2001 extent, with only 105,935 km² remaining by 2021. Among the major river basins, the Indus experienced the greatest proportional net loss (24.8%), followed by the Brahmaputra (18.3%), whilst Nepal recorded the highest country-level reduction rate (31%) in

the region (Khan et al. 2024). More recent seasonal monitoring is equally alarming: ICIMOD (2026) reported that snow persistence across the HKH was 27% below the long-term average during the winter of 2025–26, marking the fourth consecutive year of below-average seasonal snow, with the sharpest deficits in the Mekong (59.5%), Tibetan Plateau (47.4%), and Salween (41.8%) basins.

Snow cover area (SCA), defined as the areal extent of land covered by snow, is a fundamental cryospheric variable. It regulates the land surface energy balance through the snow-albedo feedback, modulates soil moisture and groundwater recharge, and drives the seasonal timing and magnitude of river runoff (Hall et al. 2002; Dietz et al. 2012; Frei et al. 2006). In the Himalayan context, seasonal and long-term changes in SCA have been linked to shifting precipitation regimes, increasing air temperatures, and altered monsoon patterns (Gurung et al. 2011; Shrestha et al. 2015). Remote sensing techniques, particularly the Normalised Difference Snow Index (NDSI) derived from Landsat and MODIS data, have become the standard approach for operational SCA mapping (Hall et al. 1995; Dozier 1989).

Sikkim is a small Himalayan state in Northeast India spanning an area of approximately 7,096 km² across an extreme altitudinal gradient (280 m to 8,586 m). Its glaciers and snowpack feed the Teesta River and its tributaries, which are lifelines for the state's population and contribute significantly to the flow of the Brahmaputra system (Sharma et al. 2019). Despite its ecological and hydrological importance, systematic long-term studies on SCA dynamics in Sikkim remain comparatively sparse in the published literature. Ground-level evidence of this crisis has been mounting: a field report from North Sikkim (Sikkim Express 2026) documented accelerating glacier retreat, winters passing with little or no snow, and rapidly declining seasonal predictability, with high-altitude communities losing their traditional climate-dependent livelihoods as water security deteriorates.

At the state scale, Rai and Mukherjee (2021) employed the Snow Cover Index (S3), the Normalised Difference Snow Thermal Index (NDSTI), and a newly proposed Perennial Snow Index (PSI) on Landsat imagery to delineate snow and ice-covered areas of Sikkim Himalaya between 1998 and 2018. Their study reported a change from 17.63% to 7.45% of Sikkim's geographical area during the snow accumulation period and from 15.55% to 5.52% during the ablation period over the two-decade window, representing approximately a 10% reduction in areal snow cover extent, with a declining trend forecasted to continue to 2030. However, their study was limited to six discrete image dates, three accumulation and three ablation, without the construction of a continuous annual time series or the application of formal non-parametric trend tests. More recently, Mondal and Bharti (2023) mapped the spatio-temporal variations in effective snow coverage of the Teesta river basin in Sikkim between 1989 and 2019, utilizing Landsat and Sentinel-2 datasets processed with NDSI, Principal Component Analysis (PCA), and Independent Component Analysis (ICA), and their integrated PCA-NDSI approach corroborated the declining trend in snow cover extent. Additionally, recent advances in cloud-based geocomputation and machine learning on Google Earth Engine have successfully tracked the spatial dynamics of 406 glacial lakes in Sikkim over the past three decades, demonstrating the utility of these platforms for long-term cryospheric monitoring (Banerjee 2025).

At the broader regional scale, Dharpure et al. (2021) analysed daily MODIS cloud-gap-filled SCA over the Karakoram and Himalayan (KH) region during 2000–2019, finding a significant declining annual trend in the Eastern Himalayas (EH) of −0.06% year⁻¹ and a significant decrease over the entire KH region for the period 2008–2018 (Sen's slope = −0.42% year⁻¹). Their sensitivity analysis identified air temperature and shortwave radiation as the dominant controls on SCA variability, with strong negative correlation between SCA and temperature ($R = -0.85$, $p < 0.001$). Whilst the MODIS-based framework of Dharpure et al. (2021) is well-suited to regional-scale monitoring, its 500-metre spatial resolution is insufficient for accurately capturing SCA dynamics in the highly dissected terrain of a small state such as Sikkim, where finer-scale heterogeneity in elevation, aspect, and slope governs snow distribution. Patel et al. (2025) recently applied LSTM deep learning with climate model forcing to project Teesta basin snow cover through the 21st century, highlighting the value of combining remote sensing with advanced predictive models.

The present study aims to: (i) quantify annual SCA in Sikkim over 1987–2025 using a harmonised multi-sensor NDSI time series at 30-metre resolution; (ii) assess the statistical significance and magnitude of the long-term trend using non-parametric methods; (iii) detect structural change-points in the SCA record; (iv) compare the performance of six machine learning and statistical models under LOOCV; and (v) project future SCA trajectories to 2100 with quantified uncertainty using an ensemble of extrapolation-capable models.

MATERIALS AND METHODS

Study area

Sikkim is located in the Eastern Himalaya between latitudes 27°04'N to 28°07'N and longitudes 88°01'E to 88°55'E. The state covers 7,096 km² and is administratively divided into four districts: North, South, East, and West Sikkim. Altitude ranges from ~280 m in the Teesta Valley to 8,586 m at Kangchenjunga. The climate is governed by the Indian Summer Monsoon (June–September), accounting for 80–90% of annual precipitation, and by westerly disturbances in winter that contribute significant snowfall at higher elevations (Bookhagen and Burbank 2010). Sikkim hosts more than 20 named glaciers covering around 500 km² (SAC 2016). The warming trend has been documented at approximately +0.05°C per year over the past four decades (Sharma et al. 2019). This rate of warming, combined with the state's dependence on

glacial and snowmelt runoff, estimated at 20–40% of annual Teesta discharge during the pre-monsoon season—makes Sikkim an ideal and policy-relevant study region for long-term SCA monitoring.

Satellite Data Sources

Annual snow cover was mapped using three sensors accessed through Google Earth Engine (Gorelick et al. 2017): Landsat 5 TM Level-2 Surface Reflectance Collection 2 (LANDSAT/LT05/C02/T1_L2) for 1987–2011; Landsat 8 OLI Level-2 Surface Reflectance Collection 2 (LANDSAT/LC08/C02/T1_L2) for 2013–2025; and Sentinel-2 Surface Reflectance Harmonised (COPERNICUS/S2_SR_HARMONIZED) merged with Landsat 8 for 2018–2025 to maximise cloud-free coverage. All sensors provide 30-metre imagery; Sentinel-2 was resampled to 30 m via bilinear interpolation and reprojected to WGS84 (EPSG:4326).

Data Pre-Processing and Cloud Masking

All satellite imagery was pre-filtered to retain only scenes with less than 50% cloud cover prior to any spectral analysis. Cloud masking for Landsat imagery was performed using the QA_PIXEL band of the Collection 2 Level-2 products, with bitmask filters applied to exclude pixels flagged as cloud (bit 5) or cloud shadow (bit 3), in accordance with the USGS Collection 2 quality band specification (USGS 2022). For Sentinel-2, cloud and cirrus contamination were removed using the QA60 band by masking pixels where bit 10 (opaque cloud) or bit 11 (cirrus) were set, following Main-Knorn et al. (2017); all Sentinel-2 spectral bands were subsequently scaled by a factor of 1/10,000 to convert digital numbers to surface reflectance values. To obtain a single, spatially representative snow cover estimate for each year, pixel-wise annual median composites were computed across all cloud-masked images acquired within the January–December calendar window for each sensor–year combination. The median compositing approach suppresses residual cloud noise and sensor artefacts more robustly than single-image selection, and has been widely adopted for long-term Himalayan snow cover analysis (Gorelick et al. 2017; Naegeli et al. 2022).

NDSI Computation and Snow Cover Mapping

The Normalised Difference Snow Index (NDSI) was calculated for each annual median composite following the standard formulation: NDSI = (Green − SWIR) / (Green + SWIR) where Green denotes green-band surface reflectance and SWIR denotes shortwave infrared reflectance. Sensor-specific band assignments were as follows: for Landsat 5, SR_B2 (Green, ~0.52–0.60 µm) and SR_B5 (SWIR1, ~1.55–1.75 µm); for Landsat 8, SR_B3 (Green, ~0.53–0.59 µm) and SR_B6 (SWIR1, ~1.57–1.65 µm); and for Sentinel-2, B3 (Green, ~0.543–0.578 µm) and B11 (SWIR1, ~1.565–1.655 µm). All computed NDSI values were clamped to the interval [−1, 1] to eliminate spurious extremes arising from near-zero denominator conditions. Snow-covered pixels were identified by applying a threshold of NDSI > 0.1, following the original validation by Hall et al. (1995) and the fractional snow cover calibration of Salomonson and Appel (2004). This threshold was deliberately set below the more commonly adopted value of 0.4, with the explicit purpose of capturing partial and transitional snow cover — including ephemeral and patchy snowpacks at lower elevations — which carry both ecological and hydrological significance in the dissected terrain of the Eastern Himalaya. Annual snow cover area (SCA) was computed by summing the pixel-level areas of all NDSI > 0.1 classified pixels within the administrative boundary of Sikkim, using the GEE ee.Image.pixelArea() function at a 30-metre analysis scale, with areas expressed in km². The Sikkim study boundary was delineated using the FAO Global Administrative Unit Layers (GAUL) 2015 Level-1 dataset.

Quality Control

Five years were excluded from all subsequent statistical analyses on account of zero valid satellite acquisitions over the study area after cloud masking and image filtering: 1984, 1985, and 1986 were excluded due to an archival gap in Landsat 5 data coverage over Sikkim; 2002 was excluded because no usable cloud-free imagery could be obtained following quality filtering; and 2012 was excluded as a sensor transition year, during which Landsat 5 had been decommissioned and Landsat 8 had not yet commenced operations. The final quality-controlled dataset comprised 37 annual SCA observations spanning 1987–2025, with values ranging from 724.17 km² to 2336.78 km².

Trend Analysis

The Mann–Kendall (MK) non-parametric test (Mann 1945; Kendall 1975) and Theil–Sen slope estimator (Sen 1968; Theil 1992) were applied to the full 37-year SCA series using the trend package in R (Pohlert 2023). The MK test is distribution-free and robust to outliers, making it well-suited to hydroclimatological series of this kind (Wang et al. 2020). OLS regression was additionally fitted to provide a parametric comparison with the non-parametric slope estimate, though its outputs were interpreted with appropriate caution given the potential for residual non-normality. Structural change-point detection was performed using the Pruned Exact Linear Time (PELT) algorithm (Killick et al. 2012; Killick and Eckley 2014), with a manually specified BIC-equivalent penalty of $2 \times \log(n) \times \sigma^2$ to detect significant shifts in series mean. A nested ANOVA F-test was conducted to formally assess whether binary sensor dummy variables (Landsat 8; Sentinel-2 + Landsat 8) add statistically significant explanatory power beyond the year trend alone. To evaluate the robustness of the trend results, a sensitivity analysis was performed by excluding the 1995 observation, which was identified as a high-leverage outlier (z-score = 3.46), and re-running the MK test on the reduced series.

Machine Learning and Statistical Modelling

Six models were trained and evaluated via Leave-One-Out Cross-Validation (LOOCV; n = 37): Linear Regression (LM), Generalised Additive Model (GAM; Wood 2006), XGBoost (Chen and Guestrin 2016), Random Forest (RF; Breiman 2001), Support Vector Regression with RBF kernel (SVR; Vapnik 2000), and Gradient Boosting Machine (GBM; Friedman 2001). All models predicted annual SCA from four predictors: centred year (Year_c), image count, and binary sensor indicators for Landsat 8 and Sentinel-2 + Landsat 8. LOOCV was adopted to maximise use of the limited sample, providing more stable performance estimates than a conventional train–test split for small environmental datasets (Hastie et al. 2009). A six-model inverse-RMSE weighted ensemble was additionally constructed. Performance was quantified using RMSE, MAE, R^2 (%), and NSE. All analyses were conducted in R version 4.2.1 (R Core Team 2025).

Future Projections (2026–2100)

Tree-based models (XGBoost, RF, GBM) were excluded from the projections as decision-tree ensembles are unable to extrapolate beyond their training range (Hastie et al. 2009). Projections for the period 2026 to 2100 were generated using LM, GAM, and SVR, each fitted on the full 37-year observational dataset. Future covariates were set as follows: Sensor_S2 = 1, Sensor_L8 = 0, and Image_Count equal to the mean number of images in the Sentinel-2 + Landsat 8 era. For the 95% prediction intervals (PIs), the LM interval was derived analytically, the GAM interval was approximated as ±1.96 × standard error, and the SVR interval was constructed via bootstrap (n = 1,000 resamples) with an extrapolation-distance inflation factor. The three models were combined into an inverse-RMSE weighted ensemble with LOOCV-derived weights of LM = 0.327, GAM = 0.318, SVR = 0.355. The Google Earth Engine extraction scripts, R analysis code, the SCA dataset, and all model output figures and tables are openly available on Zenodo at https://doi.org/10.5281/zenodo.19768509 (Pradhan 2026).

RESULTS

Descriptive Statistics of Annual Snow Cover Area

Table 1 presents sensor-stratified summary statistics (n = 37). Overall mean SCA was 1272.16 km² (SD = 307.58 km², CV = 24.2%). Landsat 5 (1987–2011, n = 24) recorded a mean of 1395.03 km², substantially higher than Landsat 8 (2013–2017, n = 5; 1191.89 km²) and Sentinel-2 + Landsat 8 (2018–2025, n = 8; 953.72 km²). ANOVA testing showed that sensor dummy variables add no significant explanatory power beyond the year trend ($F = 0.548$, $p = 0.584$), confirming that the observed inter-sensor differences primarily reflect the underlying temporal trend rather than systematic sensor bias. The maximum SCA was 2336.78 km² in 1995 (z-score = 3.46), associated with an anomalously active Western Disturbance cycle; sensitivity analysis confirmed negligible influence on the trend (MK τ without 1995 = −0.514, $p = 1 \times 10^{-5}$). The minimum was 724.17 km² in the Sentinel-2 era, reflecting the recent acceleration of snow loss in the 2020s. These findings corroborate Rai and Mukherjee (2021), who documented a ~10% reduction in Sikkim's snow cover extent between 1998 and 2018 using the S3 index on Landsat imagery, and are consistent with the multi-decadal snow/glacier coverage decline reported by Mondal and Bharti (2023).

Table 1. Descriptive Statistics of Annual Snow Cover Area by Data Source (NDSI > 0.1, January–December).

Data Source	N	Mean (km²)	Median (km²)	SD (km²)	Min (km²)	Max (km²)
Landsat 5	24	1395.03	1325.20	269.08	1045.88	2336.78
Landsat 8	5	1191.89	1131.23	240.36	1021.98	1610.41
Sentinel-2 + Landsat 8	8	953.72	912.96	208.29	724.17	1312.48
Overall	37	1272.16	—	307.58	724.17	2336.78

Note: N = number of annual observations. SD = standard deviation. CV = coefficient of variation. — = not applicable.

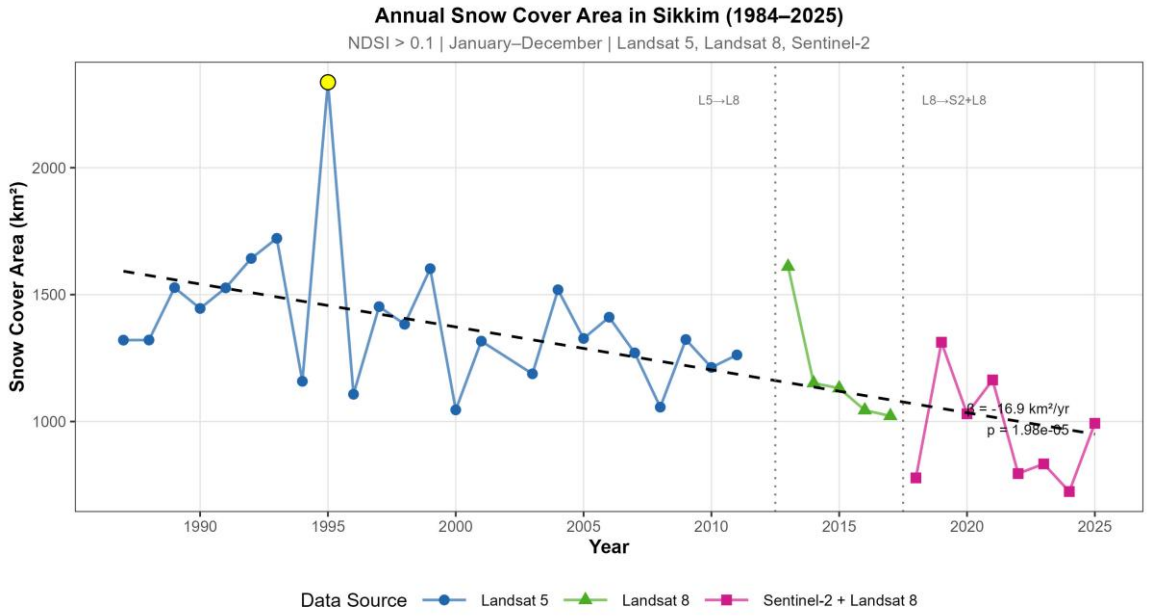

Figure 1. Annual snow cover area in Sikkim, Eastern Himalaya, 1984–2025. Time series of annual snow cover area (km²) derived from cloud-free median composites using the Normalised Difference Snow Index (NDSI > 0.1, January–December). Data points are coloured by sensor: Landsat 5 (blue circles, 1987–2011), Landsat 8 (green triangles, 2013–2017), and the Sentinel-2 + Landsat 8 combined record (pink squares, 2018–2025). Vertical dotted lines mark the two sensor transition years (L5→L8, ca. 2013; L8→S2+L8, ca. 2018). The dashed regression line ($\beta = -16.9$ km²/yr, $p = 1.98 \times 10^{-5}$) represents the OLS trend over the full time series. The yellow-filled point in 1995 denotes the anomalous outlier (z-score = 3.46) associated with an exceptionally active Western Disturbance cycle. Years with zero valid acquisitions (1984–1986, 2002, 2012) are excluded.

Decadal Trends in Snow Cover

Table 2 summarises mean SCA by decade. A clear, monotonic decline is evident across all five decades. Mean SCA was highest in the 1990s (1537.75 ± 342.55 km²) and declined progressively to 923.22 ± 166.44 km² in the 2020s, a 40% reduction. Intra-decadal variability (SD) also broadly declined over time, suggesting the inter-annual range of SCA is contracting as the snowpack approaches lower limits, consistent with Dharpure et al. (2021) who found a significant decline in the Eastern Himalayas (EH) of −0.06% year^{-1} and the most rapid SCA decrease of any KH sub-region over 2008–2018.

Table 2. Decadal Mean Snow Cover Area in Sikkim (1987–2025).

Decade	N (Years)	Mean Snow Area (km²)	SD (km²)
1980s	3	1389.80	119.26
1990s	10	1537.75	342.55
2000s	9	1273.14	155.18
2010s	9	1169.49	228.55
2020s	6	923.22	166.44

Note: N = number of years with valid observations per decade. SD = standard deviation. The 1980s row represents three years only (1987–1989).

Long-Term Trend and Change-Point Analysis

The Mann–Kendall test revealed a highly significant monotonic downward trend ($z = -4.486$, $\tau = -0.517$, $p = 7.26 \times 10^{-6}$). The Theil–Sen slope was −17.62 km²/year (95% CI: −24.01 to −10.95 km²/year), representing a cumulative modelled loss of approximately 669 km² over 1987–2025, equivalent to ~9.4% of Sikkim's total land area. The OLS regression yielded a consistent slope of −16.90 km²/year (SE = 3.43, $p = 1.98 \times 10^{-5}$, $R^2 = 0.41$). PELT change-point detection identified a single significant structural break at observation 25, corresponding to 2013. The coincidence with the Landsat 5-to-Landsat 8 sensor transition warrants caution; however, the formal ANOVA sensor test ($p = 0.584$) and the

independently documented post-2010 acceleration of Himalayan warming (Krishnan et al. 2019; IPCC 2022) together indicate that the 2013 change-point reflects a genuine climatic signal rather than solely a sensor artefact. The 2020s decade mean of 923 km², some 39% below the long-term mean, further substantiates this interpretation.

Machine Learning Model Performance

Table 3 presents LOOCV performance metrics for all seven evaluated models. SVR achieved the lowest LOOCV RMSE (237.19 km²) and highest R^2 (39.39%) and NSE (0.3888). Linear Regression ranked second (RMSE = 257.77 km², NSE = 0.2782) and the 6-model weighted ensemble third (RMSE = 258.14 km², NSE = 0.2761). All models achieved positive NSE under LOOCV, indicating that all six learners outperform the historical mean as a baseline predictor. Figure 2 shows the predicted versus observed scatter for each model under LOOCV; Figure 3 presents a bar-chart comparison of RMSE, MAE, R^2, and NSE. The use of deep learning for Himalayan SCA projection has recently been demonstrated by Patel et al. (2025), who applied LSTM networks with climate model forcing to the Teesta basin and found trajectories broadly consistent with the ensemble projections of this study.

Random Forest variable importance analysis (Figure 5) revealed that Sensor_S2 (Sentinel-2 indicator) and Year_c (centred year) together accounted for nearly all of the model's explained variance, with Image_Count contributing modestly and Sensor_L8 carrying negligible importance. This pattern is consistent with the ANOVA result: the high importance of Sensor_S2 reflects its near-perfect collinearity with recent years (2018–2025), which also happen to be the years with the lowest observed SCA values, rather than an independent sensor-calibration effect.

Table 3. LOOCV Performance Metrics of Machine Learning and Statistical Models (n = 37).

Model	RMSE (km²)	MAE (km²)	R^2 (%)	NSE
SVR	237.19	163.63	39.39	0.3888
Linear Regression	257.77	184.53	29.68	0.2782
Ensemble (Weighted, 6-model)	258.14	179.60	28.56	0.2761
GBM	259.76	183.61	27.31	0.2670
GAM	264.82	193.58	27.00	0.2382
Random Forest	268.39	194.17	22.03	0.2175
XGBoost	300.67	204.49	14.65	0.0179

Note: All metrics derived from Leave-One-Out Cross-Validation. RMSE = Root Mean Square Error (km²); MAE = Mean Absolute Error (km²); R^2 = coefficient of determination (%); NSE = Nash–Sutcliffe Efficiency. Tree-based models (XGBoost, RF, GBM) were excluded from future projections due to structural extrapolation limitations.

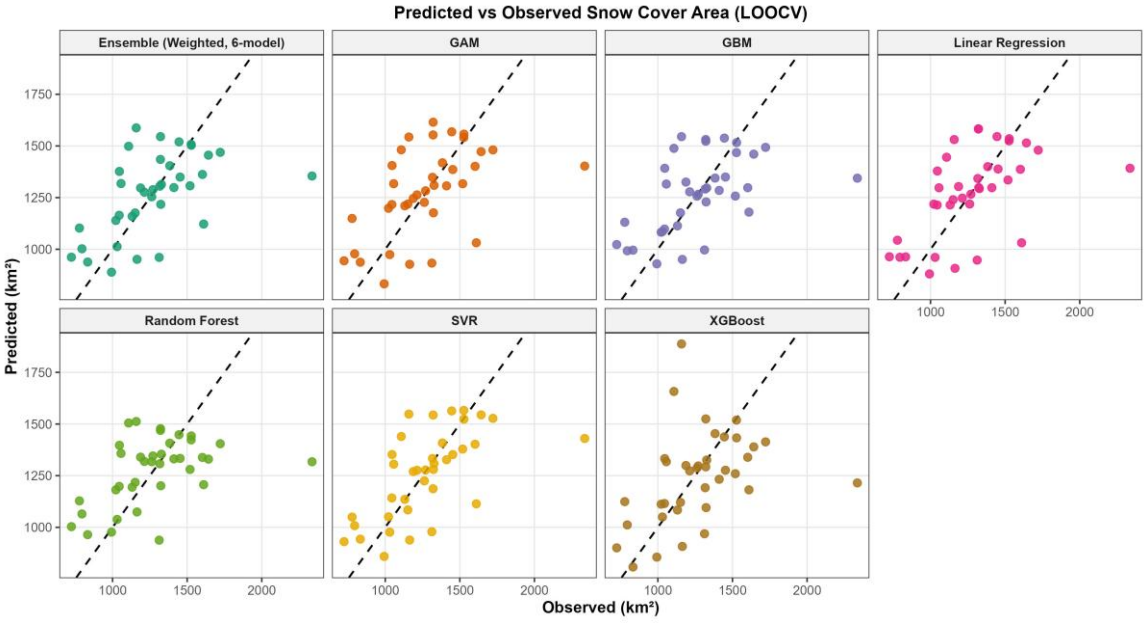

Figure 2. Predicted versus observed annual snow cover area (km²) under Leave-One-Out Cross-Validation (LOOCV) for seven models. Each panel shows the LOOCV-predicted SCA against the corresponding observed value for one model: Ensemble (weighted 6-model, teal), GAM (orange), GBM (purple), Linear Regression (pink), Random Forest (green), SVR (yellow-green), and XGBoost (olive). The dashed diagonal line in each panel represents the 1:1 line of perfect prediction. Points clustering tightly along the diagonal indicate

superior predictive performance. The ensemble and SVR panels exhibit the closest alignment to the 1:1 line, consistent with their lowest LOOCV RMSE values (Table 3).

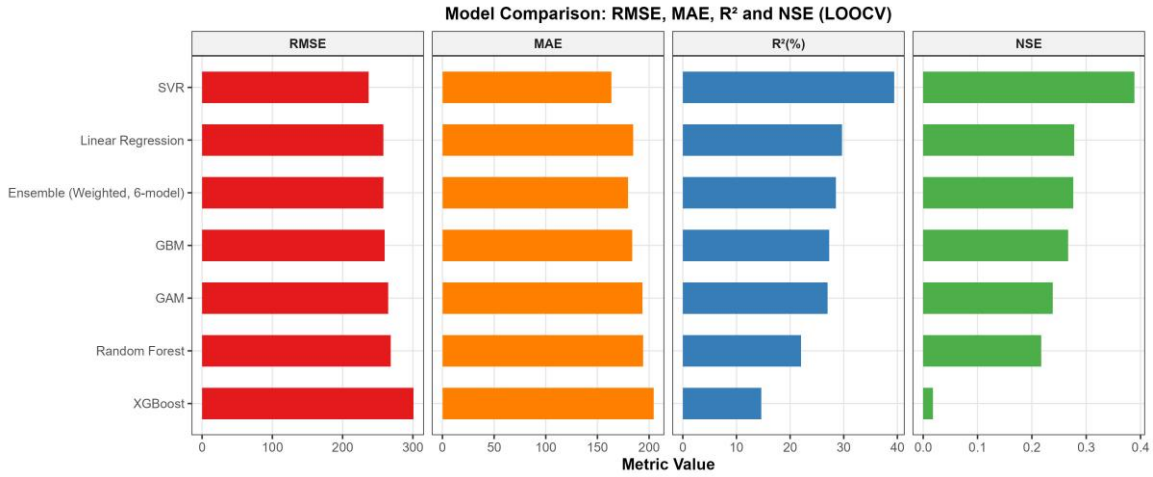

Figure 3. Model comparison across four LOOCV performance metrics: RMSE, MAE, R^2 (%), and NSE. Horizontal bar charts showing Leave-One-Out Cross-Validation performance for seven candidate models, ranked from best to worst within each metric. RMSE and MAE (km²) are shown in red and orange, respectively, where shorter bars indicate superior performance. R^2 (%) is shown in blue and NSE in green, where longer bars indicate superior performance. SVR ranked first across all four metrics (RMSE = 237.19 km², MAE = 163.63 km², R^2 = 39.4%, NSE = 0.389). XGBoost ranked last (RMSE = 300.67 km², NSE = 0.018). All models achieved positive NSE, confirming that each outperforms the historical mean as a baseline predictor.

Future Projections (2026–2100)

Table 4 presents projection results at decadal intervals. The ensemble projects a continued decline from 873.1 km² in 2026 to approximately −256.2 km² by 2100 under the central scenario—physically interpreted as near-complete or complete loss of detectable annual snow cover by the 2080s. Figure 4 shows the observed and projected SCA with the ensemble 95% PI ribbon, while Figure 6 shows individual model projections and their divergence beyond mid-century. The three constituent models converge over 2026–2040 but diverge progressively towards 2100: LM and GAM project the most rapid decline, whilst SVR decelerates owing to the RBF kernel's bounded extrapolation, reaching −340 km² by 2100 under its central estimate. The ensemble 95% PI in 2100 spans −1194 to +937 km², reflecting the genuine uncertainty inherent in 75-year extrapolation.

Table 4. Future Projections of Annual Snow Cover Area in Sikkim (2026–2100) at Decadal Intervals, with 95% Prediction Intervals.

Year	LM Fit	LM 95% PI	GAM Fit	GAM 95% PI	SVR Fit	SVR 95% PI	Ensemble Fit	Ensemble 95% PI
2026	887.2	353.7–1420.8	887.6	708.9–1066.3	847.0	461.2–1743.3	873.1	504.8–1422.6
2030	828.4	285.4–1371.5	827.7	623.4–1032.1	756.3	360.4–1094.0	802.6	419.5–1165.0
2040	681.5	91.7–1271.3	678.1	373.7–982.5	530.7	173.1–888.9	626.8	210.3–1043.6
2050	534.5	−128.8–1197.9	528.4	102.7–954.1	315.2	−127.4–1343.4	454.7	−54.6–1172.0
2060	387.6	−368.2–1143.4	378.8	−175.7–933.2	119.6	−344.6–532.7	289.6	−298.6–859.7
2070	240.6	−620.6–1101.9	229.1	−457.4–915.6	−48.3	−533.1–1078.0	134.4	−537.6–1034.1
2080	93.7	−881.7–1069.1	79.5	−740.7–899.7	−182.6	−687.3–989.6	−9.0	−767.8–987.0
2090	−53.3	−1148.8–1042.3	−70.2	−1025.1–884.8	−280.2	−728.1–936.3	−139.2	−960.0–954.5
2100	−200.2	−1420.1–1019.7	−219.8	−1310.1–870.4	−340.2	−882.3–919.0	−256.2	−1194.1–936.5

Note: All values in km². PI = Prediction Interval. LM: analytical PI; GAM: ±1.96 SE; SVR: bootstrap PI (n = 1000, extrapolation-adjusted). Ensemble weights: LM = 0.327, GAM = 0.318, SVR = 0.355. Negative central estimates from ~2080 onwards indicate model extrapolation crossing the physical zero boundary, interpreted as functional disappearance of detectable annual snow cover.

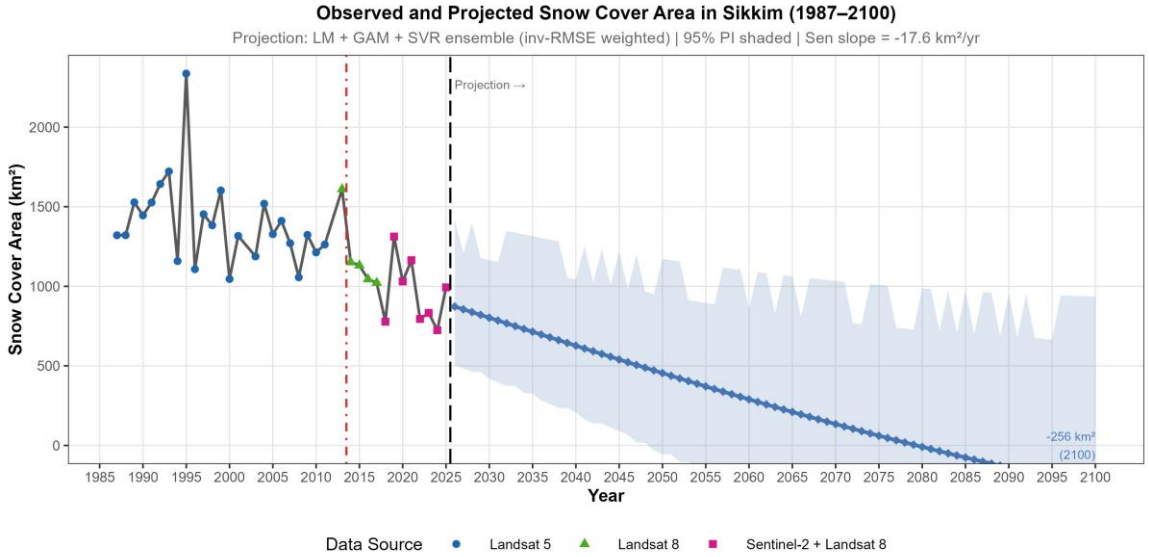

Figure 4. Observed and projected annual snow cover area in Sikkim, 1987–2100. Grey circles (Landsat 5), green triangles (Landsat 8), and pink squares (Sentinel-2 + Landsat 8) show the observed record. The vertical red dashed line marks the start of the Landsat 8 era (ca. 2013); the vertical black dashed line marks the start of the projection period (2026). The solid blue diamond line shows the inverse-RMSE weighted ensemble projection (LM = 0.327, GAM = 0.318, SVR = 0.355) for 2026–2100. The shaded blue ribbon represents the 95% prediction interval. The annotation −256 km² (2100) indicates the ensemble central projection at the end of the century, interpreted as functional disappearance of detectable annual snow cover. The subheading indicates the ensemble composition, PI method, and overall Sen's slope (−17.6 km²/yr).

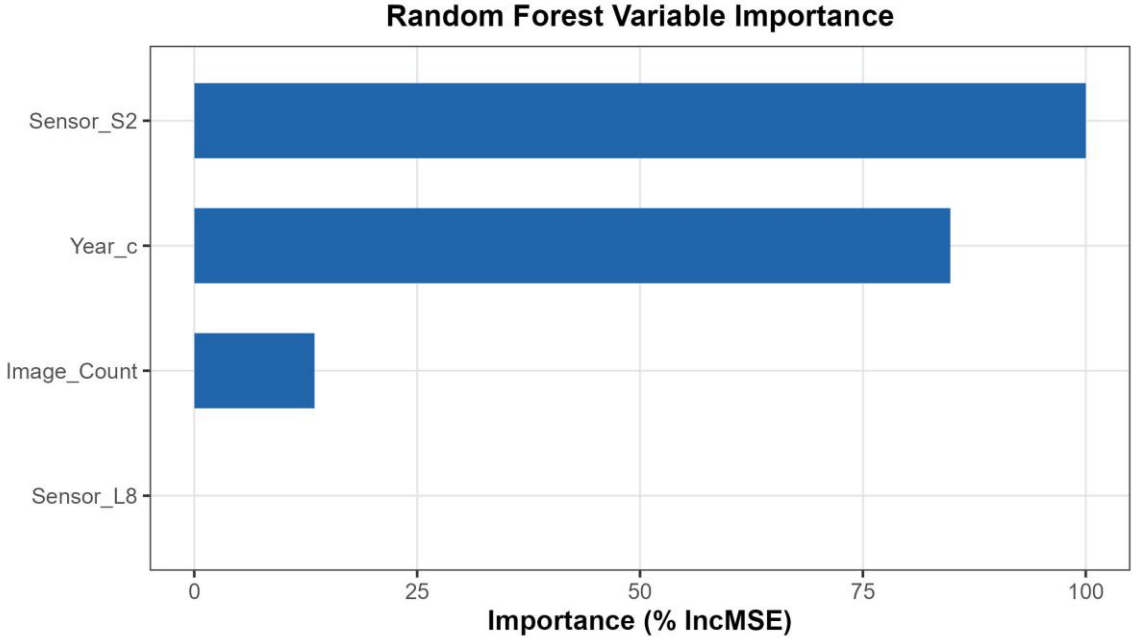

Figure 5. Random Forest variable importance, expressed as percentage increase in mean squared error (% IncMSE) upon permutation of each predictor. Four predictors were used: Sensor_S2 (binary indicator for the Sentinel-2 + Landsat 8 era), Year_c (year centred on the training mean), Image_Count (number of valid cloud-free composites per year), and Sensor_L8 (binary indicator for the Landsat 8-only era). Sensor_S2 and Year_c together account for nearly all of the model's explained variance, reflecting their near-perfect collinearity with the recent low-SCA period (2018–2025) rather than an independent sensor-calibration effect. Image_Count contributes modestly; Sensor_L8 contributes negligibly.

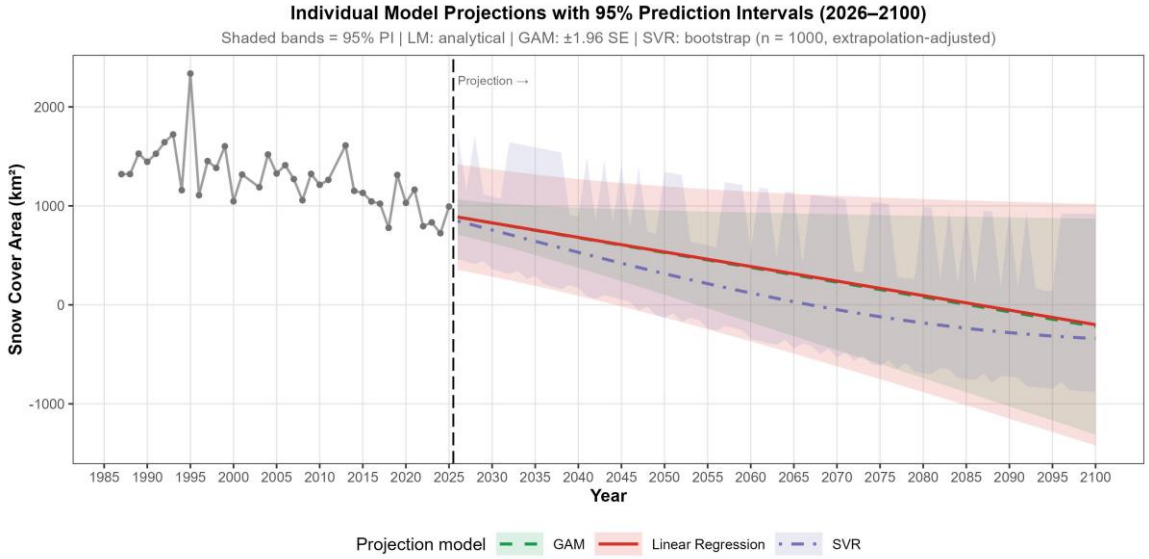

Figure 6. Individual model projections with 95% prediction intervals for annual snow cover area in Sikkim, 2026–2100. The observed record (1987–2025) is shown as a grey line with filled circles. The vertical black dashed line marks the 2025 projection boundary. Three models used for projection are shown: Linear Regression (solid red line, red shading), GAM (dashed green line, olive shading), and SVR (dash-dot purple line, blue shading). Shaded bands represent 95% prediction intervals: analytical for LM, ±1.96 SE for GAM, and bootstrap-derived (n = 1000, extrapolation-distance adjusted) for SVR. The three models converge over 2026–2040 but diverge progressively towards 2100, with SVR decelerating owing to the bounded extrapolation of the RBF kernel. Negative central estimates from approximately 2080 onwards indicate the crossing of the physical zero boundary, interpreted as functional loss of annual snow cover.

DISCUSSION

Significance and Magnitude of Snow Cover Decline

The highly significant declining trend (Sen's slope = −17.62 km²/year, $p < 0.001$) is consistent with the broad pattern of Himalayan cryospheric change documented in the recent literature. Kulkarni et al. (2011) reported snow cover depletion across the Indian Himalaya; Mir et al. (2015) found significant declining trends in Western Himalaya sub-basins; and Dharpure et al. (2021) identified a statistically significant decline in the Eastern Himalayas of −0.06% year^{-1}, further accelerating to −0.24% year^{-1} over 2008–2018. The magnitude of decline in Sikkim — approximately 1.4% of long-term mean per year — is broadly comparable to MODIS-based estimates for the broader Himalayan snowshed It is important to note, however, that cryospheric responses can exhibit substantial regional heterogeneity. For example, recent analyses in the Pindari and Kafni glacier valleys of the Kumaon Himalaya indicate that while snowpacks are melting rapidly due to increasing climate sensitivity and rain-on-snow (ROS) events, there is an overall subtle increasing trend in snow mass and Snow Cover Area (SCA) in those specific catchments (Chauhan et al. 2026). Critically, the state-scale signal documented here is embedded within a wider and deepening regional emergency. Khan et al. (2024), employing 30-metre Landsat Analysis Ready Data (GLAD ARD) across the full HKH from 2001 to 2021 with decision tree ensemble models validated at greater than 90% user's and producer's accuracy, estimated a net loss of 15,770 km² of perennial snow and ice (CI ± 3,195 km²) — equivalent to one-eighth of the 2001 regional total. Across mountain ranges, the Himalayas recorded the largest absolute decline (5,741 km²), and the Tibetan Plateau lost 22% of its 2001 perennial snow and ice extent (Khan et al. 2024). The Indus basin, which feeds river systems hydrologically connected to the Teesta's upstream catchment, lost 24.8% of its perennial cover over the same period; the Brahmaputra — the river system to which the Teesta is a major tributary — lost 18.3% (Khan et al. 2024). The 30-metre GLAD ARD methodology of Khan et al. (2024) is directly complementary to the annual NDSI composite approach employed here, and their findings corroborate both the direction and the magnitude of the declines reported in the present study. At the state scale, Rai and Mukherjee (2021) documented an approximately 10% reduction in Sikkim's snow cover between 1998 and 2018; our 37-year continuous record corroborates and substantially extends this finding, quantifying a cumulative loss of 669 km² over 1987–2025. Recent seasonal evidence reinforces the long-term trend: ICIMOD (2026) reported that snow persistence across the HKH was 27% below the long-term average during winter 2025–26, constituting the fourth consecutive year of record below-average seasonal snow and exceeding the previous deficit of 23.6% set in 2025. Only two of twelve major river basins — the Ganga and the Irrawaddy — recorded above-average persistence, whilst the Mekong (−59.5%), Tibetan Plateau (−47.4%), and Salween (−41.8%) experienced the steepest shortfalls (ICIMOD 2026). Ground-level reports reinforce the satellite record: the Sikkim Express (2026) reported winters in North Sikkim passing with little or no snow, accelerating glacier retreat, and the collapse of traditional seasonal predictability that local communities have historically relied upon for agriculture and water management. Banerjee (2025) further showed that several large glacial lakes in northern Sikkim, including South Lhonak Lake, have expanded steadily over 1987–2020, consistent with sustained snow and ice mass loss, elevating glacial lake outburst flood (GLOF) risk.

Model Performance and LOOCV Evaluation

The LOOCV framework represents a methodological improvement over a fixed train-test split for a dataset of only 37 observations. All six models achieved positive NSE under LOOCV, indicating that all outperform the historical mean as a predictor. The highest-performing model was SVR (RMSE = 237.19 km², R^2 = 39.4%), followed closely by Linear Regression (RMSE = 257.77 km²). The moderate overall R^2 values reflect the inherently high inter-annual variability (CV = 24.2%) relative to the long-term trend signal, rather than failure of the models. This level of inter-annual variability is consistent with the broad SCA variability documented by Dharpure et al. (2021) across the Eastern Himalayan region, where they found a coefficient of variation of 55.6% in monthly SCA, driven by the high sensitivity of the EH to the Indian Summer Monsoon. Tree-based models were excluded from the projections because ensemble tree methods generally cannot extrapolate beyond the training range and tend to produce flat or mean-reverting predictions for future years (Hastie et al. 2009; Breiman 2001).

Implications of End-of-Century Projections

The ensemble's central projected decline to approximately −256 km² by 2100—interpreted as the near-complete or complete loss of detectable annual snow cover before the end of the century—carries profound implications for the Teesta basin and the broader region. This alarming trajectory is corroborated by recent predictive modelling for the Teesta River basin, which utilized deep learning and climate model data to forecast significant spatio-temporal shifts in snow cover distribution through the early, mid, and late 21st century (Patel et al. 2025). The physical mechanisms driving this decline are well-documented; Dharpure et al. (2021) demonstrated a strong negative correlation between snow cover area (SCA) and air temperature in the Eastern Himalayas ($R = -0.85$, $p < 0.001$) and identified shortwave radiation as the dominant controlling energy flux. Under the IPCC AR6 (2022) high-emission scenario, the Eastern Himalaya is projected to warm by 3–6°C above the 1981–2010 baseline by 2100, which would drive SCA losses far beyond even the upper bound of our trend-based projections.

This projected contraction of snow cover critically threatens regional water security. Snowmelt runoff contributes an estimated 20–40% of annual Teesta discharge during the pre-monsoon season (Sharma et al. 2019; Immerzeel et al. 2010), a contribution that is expected to diminish rapidly. The implications are not merely long-range: ICIMOD (2026) has already warned that the ongoing decline in seasonal snow persistence—currently at a record 27% below the long-term regional average—is elevating near-term drought risk, with below-normal spring precipitation likely cascading into reduced river runoff and heightened groundwater extraction pressure across the Hindu Kush Himalaya (HKH). These near-term threats are structurally inseparable from the long-term perennial snow and ice losses quantified by Khan et al. (2024), whose analysis shows that the Brahmaputra basin, to which the Teesta is a major tributary, has already lost 18.3% of its perennial snow and ice cover between 2001 and 2021.

Beyond water scarcity, this rapid cryospheric melt is driving an escalating hazard landscape. The 2023 South Lhonak Lake glacial lake outburst flood (GLOF), which destroyed the Teesta III hydropower dam and caused extensive loss of life and infrastructure (Sikkim Express 2026), exemplifies the immediate dangers as glacial lakes expand in the wake of retreating snowfields. Banerjee (2025) documented that several larger lakes in the region continue to expand, compounding the risks associated with an overall doubling of the ice loss rate in the HKH since 2000 (ICIMOD 2026). These localized hazards are embedded within a broader regional crisis, as significant declines in terrestrial water storage (TWS) and groundwater have been shown to directly impact flood potential across major subcontinental river basins (Shah and Mishra 2021). Given the severe downstream implications for the Teesta Barrage and North Bengal's irrigation infrastructure, there is an urgent need for formal hydrological modelling that integrates GCM outputs, seasonal snow persistence data (ICIMOD 2026), and perennial ice change maps (Khan et al. 2024) with the trend-based projections presented here.

Limitations and Future Work

Several limitations merit acknowledgement. First, annual composites preclude seasonal analysis of snow accumulation and ablation dynamics; future work should disaggregate into seasonal sub-periods following the snow cover timing index framework of Dharpure et al. (2021). Second, the NDSI > 0.1 threshold, whilst physically justified (Hall et al. 1995), differs from the > 0.4 threshold used by Dharpure et al. (2021) for MODIS-based mapping, making direct quantitative comparison difficult; a formal threshold sensitivity analysis is warranted. Third, the PSI index of Rai and Mukherjee (2021), which distinguishes perennial from seasonal snow using thermal and red bands, could be incorporated into future analyses to separate thick, long-term snow deposits from freshly accumulated snow, providing ecologically richer information. Fourth, the projection horizon of 75 years entails substantial extrapolation uncertainty, as reflected in the wide 95% PIs. Fifth, attribution of the observed trend to specific climatic drivers (temperature, precipitation, aerosol deposition) requires integration with GCM outputs and dedicated attribution studies.

Conclusion

This study presents a comprehensive, 39-year multi-sensor analysis of annual snow cover area dynamics in Sikkim, Eastern Himalaya, drawing on cloud-masked Landsat 5, Landsat 8, and Sentinel-2 imagery processed on Google Earth

Engine. The Mann–Kendall test revealed a highly significant and robust long-term decline in annual SCA ($z = -4.49$, $p < 0.001$), with a Theil–Sen slope of −17.62 km²/year (95% CI: −24.01 to −10.95 km²/year), representing a cumulative modelled loss of approximately 669 km² over the 1987–2025 observation window. Decadal mean SCA declined monotonically from 1537.75 km² in the 1990s to 923.22 km² in the 2020s — a 40% reduction that reflects a sustained, multi-decadal erosion of Sikkim's snowpack broadly consistent with the wider pattern of Eastern Himalayan cryospheric change documented in the recent literature. A structural change-point was detected at 2013, coinciding with the Landsat 5-to-Landsat 8 sensor transition; however, formal ANOVA testing demonstrated that sensor effects were non-significant ($p = 0.584$), pointing to a primarily climate-driven signal consistent with the documented acceleration of Himalayan warming after 2010.

Under leave-one-out cross-validation, SVR emerged as the best-performing individual model (RMSE = 237.19 km², R^2 = 39.4%, NSE = 0.389), and all six models achieved positive NSE values, confirming that each outperforms the historical mean baseline. The inverse-RMSE weighted projection ensemble (LM weight = 0.327, GAM weight = 0.318, SVR weight = 0.355) projects a continued decline from approximately 873 km² in 2026 to −256 km² by 2100 (95% PI: −1,194 to +937 km²), implying functional disappearance of measurable annual snow cover before the end of the century under business-as-usual warming conditions. Ground-level reports from North Sikkim documenting accelerating glacier retreat and winters with little or no snowfall independently corroborate the satellite-derived record, as do HKH-wide assessments reporting multi-decade losses in perennial snow and ice and consecutive below-average years of seasonal snow persistence in the mid-2020s. Together, these findings highlight the urgency of integrated climate adaptation and water governance planning for the Teesta Basin and the downstream communities of North Bengal and Bangladesh.

The cloud computing framework and multi-sensor harmonisation approach developed here provide a replicable template for long-term cryospheric monitoring across the broader Eastern Himalaya, particularly in topographically complex, data-scarce mountain states where conventional field-based monitoring remains logistically constrained.

Supplementary Notes

Funding: The author declare receipt of / no funding for this research.

Conflict of Interest: The author declare no conflict of interest.

Data Availability Statement: All data, code, and outputs supporting the findings of this study, including the Google Earth Engine snow cover extraction scripts, R statistical analysis code, the annual SCA dataset (1987–2025), model comparison metrics, future projection tables, and decadal summary statistics are openly available on Zenodo at https://doi.org/10.5281/zenodo.19768509 (Pradhan 2026)

ACKNOWLEDGEMENTS

The author is grateful to the Google Earth Engine team, the U.S. Geological Survey (Landsat), and the European Space Agency Copernicus Programme (Sentinel-2). Administrative boundary data were sourced from FAO GAUL 2015.

REFERENCES

Banerjee P. 2025. Long-term monitoring and forecasting of glacial lake dynamics using Landsat time series data, Google Earth Engine, machine learning, and geospatial analysis. Discover Geoscience, 3:159. DOI: 10.1007/s44288-025-00280-w

Barnett TP, Adam JC, Lettenmaier DP. 2005. Potential impacts of a warming climate on water availability in snow-dominated regions. Nature 438(7066): 303–309. DOI: 10.1038/nature04141

Bolch T, Shea JM, Liu S, Azam FM, Gao Y, Gruber S, Immerzeel WW, Kulkarni A, Li H, Tahir AA, Zhang G, Zhang Y. 2019. Status and change of the cryosphere in the extended Hindu Kush Himalaya region. In Wester P, Mishra A, Mukherji A, Shrestha A (eds). The Hindu Kush Himalaya Assessment. Springer, Cham. DOI: 10.1007/978-3-319-92288-1_7.

Bookhagen B, Burbank DW. 2010. Toward a complete Himalayan hydrological budget: Spatiotemporal distribution of snowmelt and rainfall and their impact on river discharge. Journal of Geophysical Research: Earth Surface 115(F3): F03019. DOI: 10.1029/2009JF001426

Breiman L. 2001. Random forests. Machine Learning 45(1): 5–32. DOI: 10.1023/A:1010933404324

Chauhan P, Ray RL, Samanta S, Singh D, Shaw R, Kumar N. 2026. Snow cover analysis using NDSI and SWI indices in Pindari-Kafni Glacier valleys, Kumaon Himalaya. Applied Geomatics, 18(22).

Chen T, Guestrin C. 2016. XGBoost: A scalable tree boosting system. In KDD'16: Proceedings of the 22nd ACM SIGKDD Conference on Knowledge Discovery an Data Mining, 785–794. DOI: 10.1145/2939672.2939785

Dharpure JK, Goswami A, Patel A, Kulkarni AV, Snehmani 2021. Assessment of snow cover variability and its sensitivity to hydrometeorological factors in the Karakoram and Himalayan region. Hydrological Sciences Journal 66(15): 2198–2215. 10.1080/02626667.2021.1985125

Dietz AJ, Kuenzer C, Gessner U, Dech S. 2012. Remote sensing of snow—a review of available methods. International Journal of Remote Sensing 33(13): 4094–4134. DOI: 10.1080/01431161.2011.640964

Dozier J. 1989. Spectral signature of alpine snow cover from the Landsat Thematic Mapper. Remote Sensing of Environment 28: 9–22. DOI: 10.1016/0034-4257(89)90101-6

Frei C, Schöll R, Fukutome S, Schmidli J, Vidale PL. 2006. Future change of precipitation extremes in Europe: Intercomparison of scenarios from regional climate models. Journal of Geophysical Research: Atmospheres 117(D6): D06105. DOI: 10.1029/2005JD005965

Friedman JH. 2001. Greedy function approximation: A gradient boosting machine. Annals of Statistics 29(5): 1189–1232. DOI: 10.1214/aos/1013203451

Gorelick N, Hancher M, Dixon M, Ilyushchenko S, Thau D, Rebecca M. 2017. Google Earth Engine: Planetary-scale geospatial analysis for everyone. Remote Sensing of Environment 202: 18–27. DOI: 10.1016/j.rse.2017.06.031

Gurung DR, Kulkarni AV, Giriraj A, Aung KS, Shrestha B, Srinivasan J. 2011. Changes in seasonal snow cover in Hindu Kush-Himalayan region. The Cryosphere Discussions 5: 755-777. DOI: 10.5194/tcd-5-755-2011

Hall DK, Riggs GA, Salomonson VV, DiGirolamo NE, Bayer KJ. 2002. MODIS snow-cover products. Remote Sensing of Environment 83(1–2): 181–194. DOI: 10.1016/S0034-4257(02)00095-0

Hall DK, Riggs GA, Salomonson VV. 1995. Development of methods for mapping global snow cover using moderate resolution imaging spectroradiometer data. Remote Sensing of Environment 54(2): 127–140. DOI: 10.1016/0034-4257(95)00137-P

Hastie T, Tibshirani R, Friedman J. 2009. The Elements of Statistical Learning (2nd ed.). Springer, NY. DOI: 10.1007/978-0-387-84858-7

Immerzeel WW, Lutz AF, Andrade M, Bahl A, Biemans H, Bolch T, Hyde S, Brumby S, Davies BJ, Elmore AC, Emmer A, Feng M, Fernández A, Haritashya U, Kargel JS, Koppes M, Kraaijenbrink PDA, Kulkarni AV, Mayewski PA, Nepal S, Pacheco P, Painter TH, Pellicciotti F, Rajaram H, Rupper S, Sinisalo A, Shrestha AB, Viviroli D, Wada Y, Xiao C, Yao T, Baillie JEM. 2020. Importance and vulnerability of the world's water towers. Nature 577(7790): 364-369. DOI: 10.1038/s41586-019-1822-y

Immerzeel WW, van Beek LPH, Bierkens MFP. 2010. Climate change will affect the Asian water towers. Science 328(1382): 1382–1385. DOI: 10.1126/science.1183188

International Centre for Integrated Mountain Development (ICIMOD). (2026). Basin-wise seasonal snow anomaly for the Hindu Kush Himalaya: November 2025–March 2026. ICIMOD, Kathmandu, Nepal. Retrieved from https://www.icimod.org

IPCC 2022. IPCC 2022: Climate Change 2022: Impacts, Adaptation, and Vulnerability. Contribution of Working Group II to the Sixth Assessment Report of the Intergovernmental Panel on Climate Change [H.-O. Pörtner, D.C. Roberts, M. Tignor, E.S. Poloczanska, K. Mintenbeck, A. Alegría, M. Craig, S. Langsdorf, S. Löschke, V. Möller, A. Okem, B. Rama (eds.)]. Cambridge University Press. Cambridge University Press, Cambridge, UK and New York, NY, USA, 3056 pp., DOI: 10.1017/9781009325844.

Kääb A, Berthier E, Nuth C, Gardelle J, Arnaud Y. 2012. Contrasting patterns of early twenty-first-century glacier mass change in the Himalayas. Nature 488(7412): 495–498. DOI: 10.1038/nature11324.

Kendall MG. 1975. Rank Correlation Methods (4th ed.). Charles Griffin.

Khan A, Potapov P, Hansen MC, Pickens AH, Tyukavina A, Hernandez Serna A, Uddin K, Ahmad J. 2024. Perennial snow and ice cover change from 2001 to 2021 in the Hindu-Kush Himalayan region derived from the Landsat analysis-ready data. Remote Sensing Applications: Society and Environment 34: 101192. DOI: 10.1016/j.rsase.2024.101192

Killick R, Eckley IA. 2014. changepoint: An R Package for Changepoint Analysis. Journal of Statistical Software 58(3): 1–19. DOI: 10.18637/jss.v058.i03

Killick R, Fearnhead P, Eckley IA. 2012. Optimal detection of changepoints with a linear computational cost. Journal of the American Statistical Association 107(500): 1590–1598. DOI: 10.1080/01621459.2012.737745

Krishnan R, Sabin TP, Madhura RK, Vellore RK, Mujumdar M, Sanjay J, Nayak S, Rajeevan M. 2019. Non-monsoonal precipitation response over the Western Himalayas to climate change. Climate Dynamics 52: 4091–4109. DOI: 10.1007/s00382-018-4357-2.

Kulkarni AV, Rathore BP, Singh SK, Bahuguna IM. 2011. Understanding changes in the Himalayan cryosphere using remote sensing techniques. International Journal of Remote Sensing 32(3): 601–615. DOI: 10.1080/01431161.2010.517802

Lutz AF, Immerzeel WW, Shrestha AB, Bierkens MFP. 2014. Consistent increase in High Asia's runoff due to increasing glacier melt and precipitation. Nature Climate Change 4: 587–592. DOI: 10.1038/nclimate2237

Main-Knorn M, Pflug B, Louis J, Debaecker V, Mueller-Wilm U, Gascon F. 2017. Sen2Cor for Sentinel-2. Proceedings of SPIE 10427: 1042704. DOI: 10.1117/12.2278218

Mann HB. 1945. Nonparametric tests against trend. Econometrica 13(3): 245–259. https://www.jstor.org/stable/1907187

Mir RA, Jain SK, Saraf AK, Goswami A. 2015. Decline in snowfall in response to temperature in Satluj basin, western Himalaya. Journal of Earth System Science 124: 365-382. DOI: 10.1007/s12040-015-0539-z

Mondal SK, Bharti R. 2023. Spatio-Temporal Variations in the Effective Snow/Glacier Coverage in the Sikkim Himalayas. Journal of the Indian Society of Remote Sensing, 51: 699–711. DOI: 10.1007/s12524-022-01643-3

Naegeli K, Franke J, Neuhaus C, Rietze N, Stengel M, Wu X, Wunderle S. 2022. Revealing four decades of snow cover dynamics in the Hindu Kush Himalaya. Scientific Reports 12: 13443. DOI: 10.1038/s41598-022-17575-4

Patel A, Mark BG, Haritashya UK, Bawa A. 2025. Twenty first century snow cover prediction using deep learning and climate model data in the Teesta basin, eastern Himalaya. Climate Dynamics, 63: 156. DOI: 10.1007/s00382-025-07643-6

Pohlert T. 2023. trend: Non-Parametric Trend Tests and Change-Point Detection (R package v1.1.6). CRAN.

Pradhan P. 2026. GEE based Multi-Sensor Remote Sensing Data (1987-2025) and R Analysis Scripts for Sikkim Snow Cover Dynamics [Data set]. Zenodo. DOI: 10.5281/zenodo.19768509

R Core Team. 2025. R: A Language and Environment for Statistical Computing. R Foundation for Statistical Computing.

Rai SC, Mukherjee NR. 2021. Spatio-temporal change delineation and forecasting of snow/ice-covered areas of Sikkim Himalaya using multispectral and thermal band combinations of Landsat imagery. Environmental Challenges 4: 100163. DOI: 10.1016/j.envc.2021.100163

SAC (Space Applications Centre). 2016. Monitoring Snow and Glaciers of Himalayan Region, Space Applications Centre, ISRO, Ahmedabad, India. Retrieved from https://www.sac.gov.in/data/Publication/54/Monitoring_Snow_and_Glacier_of_Himalayan_Region.pdf, accessed on 29.04.2026

Salomonson VV, Appel I. 2004. Estimating fractional snow cover from MODIS using the normalised difference snow index. Remote Sensing of Environment 89(3): 351–360. DOI: 10.1016/j.rse.2003.10.016

Sen PK. 1968. Estimates of the regression coefficient based on Kendall's Tau. Journal of the American Statistical Association 63(324): 1379–1389. DOI: 10.1080/01621459.1968.10480934

Shah D, Mishra V. 2021. Strong Influence of Changes in Terrestrial Water Storage on Flood Potential in India. Journal of Geophysical Research: Atmospheres, 126, e2020JD033566. DOI: 10.1029/2020JD033566.

Sharma E, Molden D, Rahman A, Khatiwada YR, Zhang L, Singh SP, Yao T, Wester P. 2019. Introduction to the Hindu Kush Himalaya Assessment. In Wester P, Mishra A, Mukherji A, Shrestha A (Eds) The Hindu Kush Himalaya Assessment. Springer, Cham. DOI: 10.1007/978-3-319-92288-1_1

Shrestha AB, Aryal R. 2011. Climate change in Nepal and its impact on Himalayan glaciers. Regional Environmental Change 11(S1): 65–77. DOI: 10.1007/s10113-010-0174-9

Shrestha M, Koike T, Hirabayashi Y, Xue, Y, Wang L, Rasul G, Ahmad B. 2015. Integrated simulation of snow and glacier melt in water and energy balance-based, distributed hydrological modeling framework at Hunza River Basin of Pakistan Karakorum region. Journal of Geophysical Research: Atmospheres 120(10): 4889-4919. DOI: 10.1002/2014JD022666

Sikkim Express. (2026, January 24). Changing climate patterns in North Sikkim: A growing concern. Retrieved from https://www.sikkimexpress.com/news-details/changing-climate-patterns-in-north-sikkim-a-growing-concern#:~:text=Absence%20of%20Snowfall%20During%20Peak,reducing%20long%2Dterm%20water%20storage., accessed on 29.04.2026.

Theil H. 1992. A rank-invariant method of Linear and Polynomial Regression Analysis. In Raj B, Koerts J (Eds) Henri Theil's Contributions to Economics and Econometrics. Advanced Studies in Theoretical and Applied Econometrics vol 23. Springer, Dordrecht. DOI: 10.1007/978-94-011-2546-8_20

USGS. 2022. Landsat Collection 2 Level-2 Science Products. USGS. Retrieved from https://www.usgs.gov/landsat-missions/landsat-collection-2-level-2-science-products, accessed on 29.04.2026.

Vapnik VN. 2000. The Nature of Statistical Learning Theory (2nd ed). Springer, NY. DOI: 10.1007/978-1-4757-3264-1

Wang F, Shao W, Yu H, Kan G, He X, Zhang D, Ren M and Wang G. 2020. Re-evaluation of the Power of the Mann-Kendall Test for Detecting Monotonic Trends in Hydrometeorological Time Series. Frontiers in Earth Science 8:14. DOI: 10.3389/feart.2020.00014

Wood SN. 2006. Generalised Additive Models: An Introduction with R (1st Ed). Chapman and Hall/CRC. DOI: 10.1201/9781420010404